Thermodynamic calculations of oxygen self-diffusion in mixed-oxide nuclear fuels

Parfitt, DC, Cooper, MWD, Rushton, MJD, Christopoulos, S-RG, Fitzpatrick, ME & Chroneos, A

Original citation & hyperlink:
Parfitt, DC, Cooper, MWD, Rushton, MJD, Christopoulos, S-RG, Fitzpatrick, ME & Chroneos, A 2016, 'Thermodynamic calculations of oxygen self-diffusion in mixed-oxide nuclear fuels' *RSC Advances*, vol 6, pp. 74018-74027
https://dx.doi.org/10.1039/C6RA14424A

DOI 10.1039/C6RA14424A
ISSN 2046-2069

Publisher: Royal Society of Chemistry

Thermodynamic calculations of oxygen self-diffusion in mixed-oxide nuclear fuels

D. C. Parfitt,[1,a)] M. W. D. Cooper,[2] M. J. D. Rushton,[3] S.-R. G. Christopoulos,[1] M. E. Fitzpatrick,[1] A. Chroneos[1,b)]

[1]*Faculty of Engineering, Environment and Computing, Coventry University, Priory Street, Coventry CV1 5FB, United Kingdom*

[2]*Materials Science and Technology Division, Los Alamos National Laboratory, P.O. Box 1663, Los Alamos, NM 87545, USA*

[3]*Centre for Nuclear Engineering (CNE) & Department of Materials, Imperial College London, South Kensington Campus, London SW7 2AZ, United Kingdom*

Abstract

Mixed-oxide fuels containing uranium with thorium and/or plutonium may play an important part in future nuclear fuel cycles. There are, however, significantly fewer data available for these materials than conventional uranium dioxide fuel. In the present study, we employ molecular dynamics calculations to simulate the elastic properties and thermal expansivity of a range of mixed oxide compositions. These are then used to support equations of state and oxygen self-diffusion models to provide a self-consistent prediction of the behaviour of these mixed oxide fuels at arbitrary compositions.

Keywords: nuclear fuel; fluorite; self-diffusion;

[a)]Electronic mail: david.parfitt@coventry.ac.uk

[b)]Electronic mail: ab8104@coventry.ac.uk

1. Introduction

Uranium, plutonium and thorium dioxides are all of considerable interest to the nuclear industry owing to their use as nuclear fuels [1–4] either in isolation or in mixed-oxide fuels (MOx). These materials are important for the sustainability of the nuclear industry both in alternative fuel cycles for traditional light-water reactors or for advanced fuels in support of the Generation IV reactor designs. Mixed thorium and uranium based fuels benefit from higher melting points and thermal conductivity relative to pure UO_2 fuels; the mixture also provides a source of fissile isotopes which are lacking from pure ThO_2. Thorium is also greatly more abundant than uranium [1]. The use of PuO_2, directly or as a mixed fuel form, would enable a route to dispose of legacy stockpiles of plutonium-rich material.

The three stoichiometric oxides, UO_2, ThO_2 and PuO_2, and their solid solutions all share the same parent fluorite crystal structure. The diffusion of oxygen within this lattice is of fundamental importance in determining the physical properties of the fuel and is linked to the solubility and migration of fission products [5], and the recovery rate and relative tolerance of the oxides to radiation damage [6]. The accretion of oxygen point defects into planar clusters may also drive the formation of high-burn-up microstructures during reactor operation [7].

The shared symmetry and solid solubility that exists between UO_2, PuO_2 and ThO_2 crystals allows a wide range of nominal fuel compositions to be fabricated. This flexibility presents a challenge for fuel performance codes as many of the important physical and mechanical parameters will vary with metal-ion content. On a microstructural level, the fuel is even more complex as significant compositional heterogeneities exist at start of life (owing to the fabrication route) and subsequently evolve during operation due to both temperature- and irradiation-induced segregation

[8,9]. Consequently, there is a need to provide a self-consistent estimate of the effect of metal-ion content on both the elastic and defect properties of these materials.

Thermodynamic models can correlate atomic defect properties with bulk properties [10–12]. In the cBΩ model introduced by Varotsos and Alexopoulos [11,12] the defect Gibbs energy (g_i) is proportional to the isothermal bulk modulus (B) and the mean volume per atom (Ω) through a constant c. The cBΩ model has been previously employed to describe point defect processes including self-diffusion in a number of systems including oxides, semiconductors, and metals [13–21].

Oxygen self-diffusion in stoichiometric fluorite oxides is vacancy-mediated, in which the oxygen atoms exchange positions with adjacent oxygen vacancies. As a single diffusion mechanism is dominant over a wide temperature range, the cBΩ model is well suited to understanding self-diffusion in these materials. We use the model in this case to separate out the contribution to diffusion from changes in the elastic properties of the lattice between the different materials from the intrinsic defect processes that are common to all of the considered compositions. This allows us to parameterise the models for better predictive capabilities, without the need to perform many separate simulations, and also to understand the effect of mixed metal compositions upon lattice diffusion. The combination of these should enable improved predictions of the behaviour of new fuel forms and a more complete understanding of the effect of compositional heterogeneities within current fuels.

2. Methodology

2.1 Molecular dynamics

Molecular dynamics (MD) simulations have often been used to provide data on the diffusion properties of energy related materials such as MOx [3,22,23]. The recent Cooper-Rushton-Grimes (CRG) potential set [24] has been used for numerous fluorite

structured oxides and reproduces their thermomechanical and thermophysical properties and the Cauchy violation over a wide temperature range [22,25,26]. The CRG potential's fidelity in describing these properties arises from the introduction of many-body interactions to the model's description of interatomic forces. This is achieved using the embedded atom method [27]. The CRG model was successfully used in the calculation of diffusion properties in CeO_2, $U_{1-x}Th_xO_2$ and $Pu_{1-x}U_xO_2$ [22,23,28].

MD calculations in this study were performed within the Large-scale Atomic/Molecular Massively Parallel Simulator (LAMMPS) code [29]. To produce equilibrium volume and diffusion constants, the following process was used:

1. A 10×10×10 supercell of fluorite-structured $M_xN_{1-x}O_2$ (M = U, N = Pu,Th) was generated. Metal ions were randomly allocated to each cation site. The starting lattice parameter is arbitrary provided it is sufficiently close to the final equilibrium value for each pressure, temperature and composition. It was set to be 5.47Å.

2. Before commencing the dynamic part of the simulation, each ion was slightly displaced (by around 0.1Å) in a random direction from its lattice site. The initial velocities of all of the ions were set to a random value with the constraint that the overall velocity distribution conformed to a Maxwell Boltzmann distribution at an (arbitrary) temperature of 300K. Statistically-independent random seeds were used in each simulation.

3. A molecular dynamics simulation was performed in a constant pressure-temperature (NPT) ensemble. For 10ps the temperature of the thermostat was ramped from the initial value of 300K to the final value of temperature T. A subsequent 20ps was calculated with the thermostat held at T. Control of the temperature and pressure in the simulation was through a Nosé-Hoover

thermostat and barostat with relaxation times of 0.1 and 0.5ps respectively.

4. For calculation of the diffusion constant, the simulation box size was set to the average cell size over the previous 20ps. The ensemble was set to constant volume and energy (NVE) (no thermostat or barostat) and the positions and displacements of the ions were recorded over a subsequent 1ns.

This process allowed us to establish the equilibrium volume at a given composition, temperature and pressure of the system. We assume that the random selection of cation positions, and initiation of random velocities and displacements mean that these data are independent and statistically representative of the bulk crystal behaviour of the compositions at a given pressure and temperature.

To calculate the diffusivity D, we use a linear fit to the mean squared displacement:

$$\langle(\boldsymbol{r_i}(t) - \boldsymbol{r_i}(0))^2\rangle = 6Dt \qquad (1)$$

Where $\boldsymbol{r}_i(t)$ denotes the position of ion i at a time t and $\langle ... \rangle$ denotes a mean over all of the atoms of a single ion species within the simulation cell. A single value of D for each composition was fitted to data from ten statistically independent simulations under the same pressure and temperature set points in order to capture a representative average.

In order to investigate the bulk and diffusion properties of this system, we generated data at specific compositions of $M_xN_{1-x}O_2$ for M=U, N=Pu,Th and x=0.0, 0.25, 0.5, 0.75 and 1.0. To generate the thermoelastic properties, 100 simulations per compositions were run at a randomly selected set of temperatures and pressures in the range T={50,2500K} and P={–7.5, 7.5GPa}; in contrast to the diffusion calculations, only a single cation arrangement was used per P,T point, however we believe the

large number of total simulations is sufficient to provide appropriate averaging over the different cation distributions.

2.2 Equation of State

The pressure-volume-temperature data were used to fit a Rose-Vinet equation of state [30] in which a material of volume, *V*, at an equilibrium temperature, *T*, and pressure, *P*, are linked through an equation of the form:

$$P(T,X) = \frac{3B_0(T)}{X^2}(1 - X(V))\exp[\,\eta_0(T)(1 - X(V))] \quad (2)$$

Where $B_0(T)$ is the zero pressure bulk modulus as a function of temperature and the normalised length, *X(V)*, is given by:

$$X(V) = \left[\frac{V}{V_0(T)}\right]^{1/3} \quad (3)$$

Where V is the material volume, $V_0(T)$ is the zero-pressure volume as a function of temperature, and finally,

$$\eta_0(T) = \frac{3}{2}\left[\left.\frac{\partial B}{\partial P}\right|_0 (T) - 1\right] \quad (4)$$

Where $\left.\frac{\partial B}{\partial P}\right|_0 (T)$ is the pressure derivative of the bulk modulus at zero pressure as a function of temperature.

The physical origin of the Rose-Vinet Equation of State is based on splitting the volume derivative of the Helmholtz free energy, $F(V,T)$ into two terms:

$$P(V,T) = -\left(\frac{\partial F(T,V)}{\partial V}\right)_T = -\frac{dE(V)}{dV} + P_{\text{them.}}(T,V) \quad (5)$$

Where $E(V)$ is the energy of the system of atoms at zero temperature and $P_{\text{them.}}$ is a thermal pressure which tends to zero as $T \to 0$ and is observed to be only weakly dependent upon volume [30–33]. This assumption allows the pressure at a given volume and temperature to be written as two terms, one which has a common dependence on the volume of the system at a given reference temperature, T_R, and a

second that is independent of the system volume and linearly dependent upon temperature:

$$P(T,V) = P(T_R,V) + \alpha_0(T_R)B_0(T_R)(T - T_R) \qquad (6)$$

This expression is valid above a material's Debye temperature (300-400K for the mixed oxides considered here [34,35]) and in the absence of any structural phase transformations that would alter $E(V)$.

Vinet *et al* [36] have considered analytical functions that may represent the pressure isotherm $P(T_R,V)$ at a non-zero temperature and have noted that, for a wide range of solids, the following relationship holds:

$$H(T_R,X) \equiv \frac{X^2}{3(1-X)}P(T_R,X) = B_0(T_R)e^{\eta_0(T_R)(1-X)} \qquad (7)$$

Where the definition of $H(T_R, X)$ was motivated by the work of Rose *et al* [31] on the scaling laws of the cohesive energy of materials as a function of their lattice parameter and the remaining parameters are obtained from the empricial observation that a plot of $\ln(H)$ against (1-X) has an intercept of $B_0(T_R)$ and a gradient of $\eta_0(T_R)$ for many different types of materials [30].

To provide parameters for the Rose-Vinet equation of state it is necessary to select an (arbitrary) reference temperature, T_R, taken here to be 300K. It follows that the pressure can then be calculation at a point (T,V) by substitution of the pressure isotherm $P(T_R, X)$ from Equation 7 into Equation 6 to obtain:

$$P(T,X_R) = \frac{3B_0(T_R)}{X_R^2}(1 - X_R)\exp[\eta_0(T_R)(1 - X_R)] + \alpha_0(T_R)B_0(T_R)(T - T_R) \qquad (8)$$

The isothermal bulk modulus then follows from:

$$B(T,X_R) = \frac{B_0(T_R)}{X_R^2}\{2 + [\eta_0(T_R) - 1]X_R - \eta_0(T_R)X_R^2\}\exp[\eta_0(T_R)(1 - X_R)] \qquad (9)$$

And its pressure derivative,

$$\left[\frac{\partial B}{\partial P}\right](T,X_R) = \frac{4+[3\eta_0(T_R)-1]X_R+\eta_0(T_R)[\eta_0(T_R)-1]X_R^2-\eta_0^2(T_R)X_R^3}{3\left(2+[\eta_0(T_R)-1]X_R-\eta_0(T_R)X_R^2\right)} \qquad (10)$$

Where $\eta_0(T_R)$ is as defined in Equation 4, $\alpha_0(T_R)$ is the zero pressure instantaneous thermal expansion at the reference temperature and X_R is given by Equation 3 but evaluated at T=T_R:

$$X_R = \left[\frac{V}{V_0(T_R)}\right]^{1/3} \quad (11)$$

The functional form of this equation of state is more complex than the more widely used isothermal Birch-Murnaghan equation of state [37,38], however it has the significant advantage that it allows predictions of the volume of a material at an arbitrary temperature and pressure from only four parameters: the thermal expansion coefficient, volume, bulk modulus and pressure derivative of bulk modulus evaluated at zero pressure and a *single* reference temperature T_R.

In order to predict the thermodynamic properties at an arbitrary pressure and temperature we use a Levenberg–Marquardt least-squares algorithm [39,40] to fit the four parameters, $V_0(T_R)$, $B_0(T_R)$, $\left.\frac{\partial B}{\partial P}\right|_0 (T_R)$ and $\alpha_0(T_R)$ to the sets of P, V, T data generated by the simulations. From these fitted values, we can use Equations 8, 9 and 10 to predict volume, bulk modulus and the pressure derivative of the bulk modulus; thermal expansivity at temperature (instantaneous or averaged) may then be numerically calculated from the appropriate temperature derivatives of Equation 4.

2.3 Diffusion model

The vacancy-mediated oxygen self-diffusion is controlled by the Gibbs activation energy, g^{act}. Consequently, the diffusivity, D, is defined by the following relation [19]:

$$D = f a_0^2 \nu e^{-\frac{g^{act}}{k_B T}} \quad (12)$$

Where f is the diffusion correlation factor, a_0 is the lattice constant, ν is the attempt frequency and k_B is Boltzmann's constant.

In order to link the bulk and defect properties of the lattice to the resultant oxygen diffusivity we have employed the cBΩ model. In this the Gibbs defect energy g^{i} for oxygen defect formation is associated with the bulk properties of the material through [18,19]:

$$g^{\mathrm{i}} = c^{\mathrm{i}} \mathrm{B}\Omega \tag{13}$$

Where c^{i} is a scaling coefficient which is independent of temperature and pressure. Combining Eqs. (6) and (7):

$$D = f a_0^2 \nu e^{-\frac{c_{act} B\Omega}{k_B T}} \tag{14}$$

Where c_{act} is equivalent to c^{i} in the event that only a single defect process contributes to the overall diffusivity. The pre-exponential factor ($f a_0^2 \nu$) is dependent upon the diffusion mechanism, the crystal structure and the attempt frequency. The cBΩ model is appropriate when considering pressure and temperature variations as it encapsulates anharmonic effects exhibited by the expansion of the lattice and decrease in bulk modulus with temperature.

3. Results and Discussion

3.1 Equation of State

The Rose-Vinet equation of state was fitted to the MD data generated at each of the three end members and three intermediate compositions $U_xTh_{1-x}O_2$ and $U_xPu_{1-x}O_2$ (x=0.25, 0.5, 0.75). The fitted results for the bulk modulus, derivative of the bulk modulus and thermal expansivity are reported in Table 1. The use of these values, in association with the equations given in Section 2, allows the thermoelastic properties of each composition to be estimated at temperatures and pressures below the superionic transition. The empirical potentials used in the present study are designed to accurately reproduce the elastic properties of the matrix, so it is unsurprising that the data agree well with previous studies for the binary oxides. However the use of

statistically-averaged ternary compositions (e.g. $U_xPu_{1-x}O_2$), and the simultaneous treatment of volume and temperature in the Rose-Vinet equation of state, allow predictions of volume at an arbitrary composition, pressure and temperature.

In Figure 1, data are shown for the thermal expansion and compressibility of two example systems, UO_2 and a mixture $U_{0.5}Th_{0.5}O_2$. These data are not included in the original fit dataset but it can be seen that the equation of state does an excellent job of describing the variation in volume within the range of the fitted data. At high temperatures (greater than 2500K) there is evidence in Figure 1 of the onset of the superionic transition, which marks the beginning of significant anion disorder in the lattice. The equation of state is not fitted to data greater than 2500K, and if it were, it is not capable of capturing the discontinuous change in thermal expansion that occurs at this transition.

The bulk modulus of a theoretical mixed oxide system $M_xN_{1-x}O_2$ with complete solid solubility is given by [19],

$$B(x) = B_N \frac{f(x)}{g(x)} \tag{15}$$

Where,

$$f(x) = 1 + x\left[\left(\frac{V_M}{V_N}\right) - 1\right] \tag{16}$$

$$g(x) = 1 + x\left[\left(\frac{B_N V_M}{B_M V_N}\right) - 1\right] \tag{17}$$

And $B_{M,N}$ and $V_{M,N}$ refer to the bulk moduli and equilibrium volumes of the end members MO_2 and NO_2. Figure 2 shows a plot of the values of bulk modulus calculated from the Rose-Vinet equation of state and those predicted from the theoretical expression. The agreement is excellent, indicating that simple expressions such as the above are suitable for accounting for the variation in properties as a function of composition in these systems.

The pressure derivative of the bulk modulus as a function of composition can then be found from Equation 9 as:

$$\frac{\mathrm{d}B(x)}{\mathrm{d}P} = B'_N \frac{f(x)}{g(x)} + B_N \frac{f'(x)g(x) - f(x)g'(x)}{g(x)^2} \quad (18)$$

Where $f'(x)$ and $g'(x)$ are the pressure derivatives of $f(x)$ and $g(x)$ given by,

$$f'(x) = x \frac{V_M}{V_N} \left(\frac{1}{B_M} - \frac{1}{B_N} \right) \quad (19)$$

$$g'(x) = x \frac{V_M B_N}{V_N B_M} \left(\frac{1 - B'_M}{B_M} - \frac{1 - B'_N}{B_N} \right) \quad (20)$$

And $B'_{M,N}$ are the pressure derivatives of the bulk modulus of the end members MO_2 and NO_2. Again the fitted derivative of the isothermal pressure derivative of bulk modulus is shown in Figure 2 against the theoretical expression for $\left(\frac{\partial B}{\partial P}\right)_T(x)$ given above. The agreement is reasonable and therefore we argue that the elastic properties at an arbitrary composition are well-represented by Equations 9 and 12.

The final term in the Rose-Vinet equation of state is the thermal expansivity. In Figure 3 we show the variation in linear thermal expansion at zero pressure defined as:

$$\frac{\Delta L(T)}{L(T_R)} = \frac{V(T)^{1/3} - V(T_R)^{1/3}}{V(T_R)^{1/3}} \quad (21)$$

This is shown across the different compositions indicating that the compositional variation is relatively minor for the PuO_2-UO_2 system but greater for ThO_2-UO_2. The difference also becomes progressively greater when considering the higher temperature data in agreement with experimental reports [41].

In order to better compare with literature data on the thermal behaviour, we have also calculated the average change in linear thermal expansivity as:

$$\langle \alpha_L(T, T_R) \rangle = \frac{\Delta L(T)}{L(T_R)} \times \frac{1}{T - T_R} \quad (22)$$

This is plotted for T=1600K in Figure 3(b).

Experimental data showing the changes in thermal expansivity with composition are compared with the model predictions in Figure 3(a) and (b). We have selected the data from Reference [41] for comparison with the change in thermal expansivity at 873K and 1173K and the data from Reference [42] and originally reported by Anthonysamy *et al* [43] Tyagi *et al* [44,45] and Lynch and Beals [46] for comparison with the average linear thermal expansivity between 293K and 1600K.

The experimental data for thermal expansivity of the mixed ThO_2-UO_2 system is scattered, particularly when averaged over large temperature ranges as seen in Figure 3(b); this is likely due to either heterogeneities in material microstructure or significant deviations from stoichiometry as a function of temperature. The absolute values of average thermal expansivity are however consistent with the models and the trends are similar within each dataset. In particular, both the models and experimental data support a non-linear increase in thermal expansivity with the addition of uranium into ThO_2 which is not mirrored in the PuO_2-UO_2 system.

The fitted value of (volumetric) thermal expansivity at the reference temperature of 300K is also shown in Figure 3(c). The change mimics the trends of thermal expansion, although the differences in absolute values of expansion are only evident at high temperatures.

In the case of thermal expansivity, no general theory of variation with composition was apparent and so we fit these data using a polynomial function of the form:

$$\alpha(x, T_{\mathrm{R}}) = \sum_{n=0}^{N} a_n x^n \qquad (23)$$

Where we use a second-order polynomial (N=2) for the $Th_{1-x}U_xO_2$ system and a first-order (i.e. linear) polynomial (N=1) for the $Pu_{1-x}U_xO_2$ system, with the added constraint that the two sets of polynomials should be equal at x=0 (i.e. the common UO_2 end

member). The orders of the polynomial functions were chosen to be the simplest possible curves that adequately captured the variability in the data and trial functions with higher order coefficients did not markedly improve the fit. Fitting parameters are reported in Table 2.

3.2 Oxygen Self-Diffusion

In previous studies, the link between atomic parameters and the diffusivity of UO_2, PuO_2 and ThO_2 end-members was established [13,14] using the mean value method [47–49]. In principle, further equations could be determined for each U-Th-Pu composition. However, to avoid a proliferation of different terms, we fit the data using a universal value for the pre-exponential and making the activation coefficient compositionally dependent, i.e. fitting an equation of the form,

$$D_{cB\Omega}(M_xN_{1-x}O_2) = D_0 e^{\frac{-c_{act}(x)B\Omega}{k_BT}} \quad (24)$$

Where c_{act} is allowed to vary depending on the composition of the oxide and B and Ω are calculated from the Rose-Vinet equation of state.

Similarly to the case of thermal expansion, there is no general expression for the variability of activation coefficient with composition and so we fit the data using a second set of polynomial expressions of the form:

$$c_{act}(x) = \sum_{n=0}^{N} a_n x^n \quad (25)$$

We apply the same logic to the fitting of the thermal expansivity data, however because of the greater variability of the c_{act} parameter and the increased sensitivity of the final diffusion coefficient, a fourth-order polynomial (N=4) is used for the ThO_2-UO_2 system and a third-order (N=3) polynomial for the PuO_2-UO_2 system. Fitted values are reported in Table 2.

The results of these simulation data at each composition and the fitted polynomial functions are shown in Figure 4. The activation coefficient varies

smoothly and systematically with composition; this behaviour is monotonic in the PuO_2-UO_2 system representing an increase in oxygen diffusivity as Pu content is increased [22]. However, in the case of the ThO_2-UO_2 system there is a pronounced minimum in the activation coefficient coincident with the maximum in oxygen ion diffusivity from molecular dynamics simulations. This curious feature was previously discussed by Cooper *et al* [23] where it was attributed to the existence of Frenkel pair formation enthalpies in the mixed system that lay below those of either of the end members. Figure 4 of Reference 23 shows this splitting of the vacancy formation enthalpy demonstrating this effect.

3.3 Combined Model

Using the results of the activation coefficient fitting and the Rose-Vinet equation of state, we now summarise the model coefficients which can be used to predict the oxygen ion self-diffusion and elastic properties at an arbitrary composition in the $Th_{1-x}U_xO_2$ or $Pu_{1-x}U_xO_2$ phase diagram. The Rose-Vinet Equation of State and cBΩ diffusion model parameters are as follows:

- **Volume**, $V_0(T_R, x)$, linear interpolation between end members.
- **Bulk Modulus**, $B_0(T_R, x)$, Equation 15.
- **Pressure Derivative of Bulk Modulus**, $\left.\frac{\partial B}{\partial P}\right|_0 (T_R, x)$, Equation 18.
- **Thermal Expansivity**, $\alpha_0(T_R, x)$, polynomial fit using coefficients in Table 2.
- **Activation Coefficient**, $c_{act}(x)$, polynomial fit using coefficients in Table 2.

These values can then be used in association with Equations 8-10 in order to predict the elastic properties and oxygen ion self-diffusivity at an arbitrary pressure, temperature and volume. We show an example of this use of this model in Figure 5

which compares the volume and diffusivity values calculated from MD simulations for both the PuO_2-UO_2 and ThO_2-UO_2 systems with those predicted from the combined model.

3.4 Application to Other Systems

In addition to the properties at different temperatures, it is also of note that through the use of the cBΩ model the predictions of oxygen self-diffusion are equally applicable to a range of pressures. Therefore, these models should also account for the elastic properties and oxygen migration in mixed oxide regions subject to significant compressive or tensile stress. The stresses investigated in this paper are far above those encountered as a macroscopic stress in a nuclear fuel pin; however they would be useful in investigating diffusion around microstructural defects. For example, they may be help account for the enhanced diffusion close to dislocation cores (where elastic deformation in the surrounding lattice can lead to significant levels of strain) [50,51]. Equally, greatly enhanced diffusion has also been reported in similar fluorite-structured materials in which compositionally distinct regions lead to the generation of significant interface strains [52–55].

These results would also be applicable to modelling oxide corrosion layers formed on metallic uranium, plutonium or thorium. In these cases, the oxide layers are formed under significant compressive stresses due to the mismatch in lattice parameter between the oxide and the underlying metal substrate. Oxygen transport through these layers is one of the controlling factors that determine the overall oxidation rate.

The validation of these models is problematic due to the difficulty and expense of obtaining experimental data on these systems; the scatter in experimental values in Figure 3(b) being a pertinent illustration. Whilst experimental data remains the sole

test of scientific truth, the use of *ab initio* methods coupled with molecular dynamics may in the future enable these calculations to be replicated with density functional theory. These would reduce the number of fitted parameters in the empirical potentials through an appeal to the sounder theoretical basis of non-relativistic quantum mechanics. Calculation on $LiGe_2(PO_4)_3$ [56] have shown the use of these types of simulations in obtaining self-diffusion coefficients similar to those obtained here and these have also successfully replicated diffusion coefficients and relatively subtle chemistry effects in uranium-containing molten salt reactions [57]. These techniques are however computationally expensive, particularly for UO_2 where subtle correlations between the uranium ion *f*-electrons can confound the identification of the true ground state electronic structure [58–60].

Conclusions

In this paper we have examined the link between the composition of mixed oxide fuels, their bulk elastic properties and the value of oxygen self-diffusion. This has provided a predictive model of the elastic properties for the mixed oxides together with an estimate of the oxygen ion self-diffusion.

The addition of UO_2 into PuO_2 produces a mixed oxide which exhibits thermoelastic properties and oxygen self-diffusion values which are in-line with the average properties. In particular, the changes in elastic properties and thermal expansion are small, and captured by simple interpolation between the two end members. There is a noticeable non-linearity in the oxygen self-diffusion coefficient at high temperature; however this is bounded by the maximum value in PuO_2. The behaviour of the ThO_2-UO_2 system is more interesting in that there is a substantial difference in properties between the two end members *and* the mixed oxide exhibits properties that are poorly predicted by linear interpolation between them. This is most

dramatic in the oxygen self-diffusion coefficients, but also evident in the thermal expansivity where a simple linear average between the two end-members may significantly under-predict the calculated values.

This combined model can be used to predict volume changes, elastic properties, thermal expansion and oxygen-ion self-diffusion as a function of stress, temperature and composition. As well as investigating the effect of heterogeneity in fuels, this may also offer insight into the behaviour of the material around microstructural features that impose significant lattice strain, for example edge dislocations, gas bubbles or metal-oxide interfaces.

Acknowledgements

MWDC is funded by the Department of Energy (DoE), Office for Nuclear Energy, Nuclear Energy Advanced Modelling and Simulation (NEAMS) program. SRGC, MEF and AC are grateful for funding from the Lloyd's Register Foundation, a charitable foundation helping to protect life and property by supporting engineering-related education, public engagement and the application of research.

References

[1] M. Lung, O. Gremm, Perspectives of the thorium fuel cycle, Nucl. Eng. Des. 180 (1998) 133–146. doi:10.1016/S0029-5493(97)00296-3.

[2] W.E. Lee, M. Gilbert, S.T. Murphy, R.W. Grimes, Opportunities for Advanced Ceramics and Composites in the Nuclear Sector, J. Am. Ceram. Soc. 96 (2013) 2005–2030. doi:10.1111/jace.12406.

[3] M. Stan, Discovery and design of nuclear fuels, Mater. Today. 12 (2009) 20–28. doi:10.1016/S1369-7021(09)70295-0.

[4] M. Kazimi, Thorium Fuel for Nuclear Energy An unconventional tactic might one day ease concerns that spent fuel could be used to make a bomb, Am Sci. 91 (2003) 408–15. doi:10.1511/2003.5.408.

[5] M. Bertolus, M. Freyss, B. Dorado, G. Martin, K. Hoang, S. Maillard, et al., Linking atomic and mesoscopic scales for the modelling of the transport properties of uranium dioxide under irradiation, J. Nucl. Mater. 462 (2015) 475–495. doi:10.1016/j.jnucmat.2015.02.026.

[6] K.E. Sickafus, R.W. Grimes, J.A. Valdez, A. Cleave, M. Tang, M. Ishimaru, et al., Radiation-induced amorphization resistance and radiation tolerance in structurally related oxides., Nat. Mater. 6 (2007) 217–23. doi:10.1038/nmat1842.

[7] T. Ichinomiya, B.P. Uberuaga, K.E. Sickafus, Y. Nishiura, M. Itakura, Y. Chen, et al., Temperature accelerated dynamics study of migration process of oxygen defects in UO_2, J. Nucl. Mater. 384 (2009) 315–321. doi:10.1016/j.jnucmat.2008.12.040.

[8] H. Kleykamp, Post-irradiation studies on LWR-MOX fuel fabricated by the optimized co-milling process, J. Nucl. Mater. 324 (2004) 198–202. doi:10.1016/j.jnucmat.2003.10.004.

[9] G. Oudinet, I. Munoz-Viallard, L. Aufore, M.-J. Gotta, J.M. Becker, G. Chiarelli, et al., Characterization of plutonium distribution in MIMAS MOX by image analysis, J. Nucl. Mater. 375 (2008) 86–94. doi:10.1016/j.jnucmat.2007.10.013.

[10] J. Philibert, Some Thoughts and/or Questions about Activation Energy and Pre-Exponential Factor, Defect Diffus. Forum. 249 (2006) 61–72. doi:10.4028/www.scientific.net/DDF.249.61.

[11] P. Varotsos, K. Alexopoulos, Estimation of the migration enthalpy and entropy for cation vacancy motion in alkali halides with the NaCl-type structure, Phys. Rev. B. 15 (1977) 2348–2351. doi:10.1103/PhysRevB.15.2348.

[12] P. Varotsos, K. Alexopoulos, Calculation of the formation entropy of vacancies due to anharmonic effects, Phys. Rev. B. 15 (1977) 4111–4114. doi:10.1103/PhysRevB.15.4111.

[13] A. Chroneos, R.V. Vovk, Modeling self-diffusion in UO_2 and ThO_2 by connecting point defect parameters with bulk properties, Solid State Ionics. 274 (2015) 1–3. doi:10.1016/j.ssi.2015.02.010.

[14] A. Chroneos, M.E. Fitzpatrick, L.H. Tsoukalas, Describing oxygen self-diffusion in PuO_2 by connecting point defect parameters with bulk properties, J. Mater. Sci. Mater. Electron. 26 (2015) 3287–3290. doi:10.1007/s10854-015-2829-2.

[15] P.A. Varotsos, Calculation of point defect parameters in diamond, Phys. Rev. B. 75 (2007) 172107. doi:10.1103/PhysRevB.75.172107.

[16] E.S. Skordas, Comment on "LiH as a Li^+ and H^- ion provided by Khang Hoang, Chris G. Van de Walle, Solid State Ionics 253 (2013) 53," Solid State

Ionics. 261 (2014) 26–27. doi:10.1016/j.ssi.2014.04.001.
[17] F. Vallianatos, V. Saltas, Application of the cBΩ model to the calculation of diffusion parameters of He in olivine, Phys. Chem. Miner. 41 (2013) 181–188. doi:10.1007/s00269-013-0636-y.
[18] P. Varotsos, Comparison of models that interconnect point defect parameters in solids with bulk properties, J. Appl. Phys. 101 (2007) 123503. doi:10.1063/1.2745359.
[19] P.A. Varotsos, K.D. Alexopoulos, Thermodynamics of point defects and their relation with bulk properties, North-Holland, 1986.
[20] V. Saltas, F. Vallianatos, Thermodynamic calculations of self- and hetero-diffusion parameters in germanium, Mater. Chem. Phys. 163 (2015) 507.
[21] V. Saltas, A. Chroneos, F. Vallianatos, A thermodynamic approach of self- and hetero-diffusion in GaAs: connecting point defect parameters with bulk properties, RSC Adv. 6 (2016) 53324.
[22] M.W.D. Cooper, S.T. Murphy, M.J.D. Rushton, R.W. Grimes, Thermophysical properties and oxygen transport in the $(U_x,Pu_{1-x})O_2$ lattice, J. Nucl. Mater. 461 (2015) 206–214. doi:10.1016/j.jnucmat.2015.03.024.
[23] M.W.D. Cooper, S.T. Murphy, P.C.M. Fossati, M.J.D. Rushton, R.W. Grimes, Thermophysical and anion diffusion properties of $(U_x,Th_{1-x})O_2$, Proc. R. Soc. A Math. Phys. Eng. Sci. 470 (2014) 20140427–20140427. doi:10.1098/rspa.2014.0427.
[24] M.W.D. Cooper, M.J.D. Rushton, R.W. Grimes, A many-body potential approach to modelling the thermomechanical properties of actinide oxides., J. Phys. Condens. Matter. 26 (2014) 105401. doi:10.1088/0953-8984/26/10/105401.
[25] M.W.D. Cooper, R.W. Grimes, M.E. Fitzpatrick, A. Chroneos, Modeling oxygen self-diffusion in UO_2 under pressure, Solid State Ionics. 282 (2015) 26–30. doi:10.1016/j.ssi.2015.09.006.
[26] M.W.D. Cooper, S.C. Middleburgh, R.W. Grimes, Modelling the thermal conductivity of $(U_xTh_{1-x})O_2$ and $(U_xPu_{1-x})O_2$, 466 (2015) 29–35. doi:10.1016/j.jnucmat.2015.07.022.
[27] M.S. Daw, M.I. Baskes, Embedded-atom method: Derivation and application to impurities, surfaces, and other defects in metals, Phys. Rev. B. 29 (1984) 6443–6453. doi:10.1103/PhysRevB.29.6443.
[28] M.J.D. Rushton, A. Chroneos, Impact of uniaxial strain and doping on oxygen diffusion in CeO_2, Sci. Rep. 4 (2014) 6068. doi:10.1038/srep06068.
[29] S. Plimpton, Fast Parallel Algorithms for Short – Range Molecular Dynamics, J. Comput. Phys. 117 (1995) 1–19. doi:10.1006/jcph.1995.1039.
[30] P.Vinet, J.R. Smith, J. Ferrante, J.H. Rose, Temperature effects on the universal equation of state, Phys. Rev. B. 35 (1987) 1945–1953. doi:10.1103/PhysRevB.35.1945.
[31] J.H. Rose, J.R. Smith, F. Guinea, J. Ferrante, Universal features of the equation of state of metals, Phys. Rev. B. 29 (1984) 2963–2969. doi:10.1103/PhysRevB.29.2963.
[32] O.L. Anderson, A universal thermal equation-of-state, J. Geodyn. 1 (1984) 185–214. doi:10.1016/0264-3707(84)90027-9.
[33] M.S. Anderson, C.A. Swenson, Experimental equations of state for cesium and lithium metals to 20 kbar and the high-pressure behavior of the alkali metals, Phys. Rev. B. 31 (1985).
[34] G. Dolling, R.A. Cowley, A.D.B. Woods, The Crystal Dynamics of Uranium

Dioxide, http://dx.doi.org/10.1139/p65-135. (2011).
[35] I.J. Fritz, Elastic properties of UO_2 at high pressure, J. Appl. Phys. 47 (1976) 4353. doi:10.1063/1.322438.
[36] P.Vinet, J.R. Smith, J. Ferrante, J.H. Rose, Temperature effects on the universal equation of state, Phys. Rev. B Condens. Matter. 35 (1987) 1945–1953.
[37] F. Birch, Finite Elastic Strain of Cubic Crystals, Phys. Rev. 71 (1947) 809–824. doi:10.1103/PhysRev.71.809.
[38] F.D. Murnaghan, The Compressibility of Media under Extreme Pressures., Proc. Natl. Acad. Sci. U. S. A. 30 (1944) 244–247. doi:10.1073/pnas.30.9.244.
[39] K. Levenberg, A Method for the Solution of Certain Non-Linear Problems in Least Squares, Q. Appl. Math. 2 (1944) 164–168.
[40] D. Marquardt, An Algorithm for Least-Squares Estimation of Nonlinear Parameters, SIAM J. Appl. Math. 11 (1963) 431.
[41] A.K. Sengupta, J. Banerjee, R.K. Bhagat, R. Ramachandran, S. Majumdar, R. Division, Thermal Expansion Data of $(Th,U)O_2$ Fuels, BARC/2000/E/008. (2000).
[42] K. Bakker, E.H.P. Cordfunke, R.J.M. Konings, R.P.C. Schram, Critical evaluation of the thermal properties of ThO_2 and $Th_{1-y}U_yO_2$ and a survey of the literature data on $Th_{1-y}Pu_yO_2$, J. Nucl. Mater. 250 (1997) 1–12.
[43] S. Anthonysamy, G. Panneerselvam, S. Bera, S. V Narasimhan, P.R. Vasudeva Rao, Studies on thermal expansion and XPS of urania+thoria solid solutions, J. Nucl. Mater. 281 (2000) 15–21.
[44] A.K. Tyagi, M.D. Mathews, B.R. Ambekar, R. Ramachandran, Thermal expansion of ThO_2 4 and 6 wt.% UO_2 by HT-XRD, Thermochim. Acta. 421 (2004) 69–71.
[45] A.K. Tyagi, M.D. Mathews, Thermal expansion of ThO_2 wt% UO_2 by HT-XRD, J. Nucl. Mater. 278 (2000) 123–125.
[46] E.D. Lynch, R.J. Beals, Argonne National Laboratory, Annual Report ANL-6677, 1962.
[47] B.-H. Zhang, X.-P. Wu, Diffusion of aluminum in MgO: A thermodynamic approach study, Chinese Phys. B. 22 (2013) 056601. doi:10.1088/1674-1056/22/5/056601.
[48] B. Zhang, X. Wu, Calculation of self-diffusion coefficients in diamond, Appl. Phys. Lett. 100 (2012) 051901. doi:10.1063/1.3680600.
[49] B. Zhang, Calculation of self-diffusion coefficients in iron, AIP Adv. 4 (2014) 017128. doi:10.1063/1.4863462.
[50] S.T. Murphy, E.E. Jay, R.W. Grimes, Pipe diffusion at dislocations in UO_2, J. Nucl. Mater. 447 (2014) 143–149. doi:10.1016/j.jnucmat.2013.12.029.
[51] D.C. Parfitt, C.L. Bishop, M.R. Wenman, R.W. Grimes, Strain fields and line energies of dislocations in uranium dioxide., J. Phys. Condens. Matter. 22 (2010) 175004. doi:10.1088/0953-8984/22/17/175004.
[52] N. Sata, K. Eberman, K. Eberl, J. Maier, Mesoscopic fast ion conduction in nanometre-scale planar heterostructures., Nature. 408 946–9. doi:10.1038/35050047.
[53] X.X. Guo, I. Matei, J.-S. Lee, J. Maier, Ion conduction across nanosized CaF_2/BaF_2 multilayer heterostructures, Appl. Phys. Lett. 91 (2007) 103102. doi:10.1063/1.2779254.
[54] J. Garcia-Barriocanal, A. Rivera-Calzada, M. Varela, Z. Sefrioui, E. Iborra, C. Leon, et al., Colossal ionic conductivity at interfaces of epitaxial

ZrO_2:Y_2O_3/$SrTiO_3$ heterostructures, Science (80). 321 (2008) 676–680. doi:10.1126/science.1156393.
[55] M.J.D. Rushton, A. Chroneos, Impact of uniaxial strain and doping on oxygen diffusion in CeO_2, Sci. Rep. 4 (2014) 2–7. doi:10.1038/srep06068.
[56] J. Kang, H. Chung, C. Doh, B. Kang, B. Han, Integrated study of first principles calculations and experimental measurements for Li-ionic conductivity in Al-doped solid-state $LiGe_2(PO_4)_3$ electrolyte, J. Power Sources. 293 (2015) 11–16.
[57] C. Kwon, J. Kang, W. Kang, D. Kwak, B. Han, First principles study of the thermodynamic and kinetic properties of U in an electrorefining system using molybdenum cathode and LiCl-KCl eutectic molten salt, Electrochim. Acta. 195 (2016) 216–222.
[58] Emerson Vathonne, Julia Wiktor, Michel Freyss, Gérald Jomard and Marjorie Bertolus, DFT+U investigation of charged point defects and clusters in UO_2, J. Phys. Condens. Matter. 26 (2014) 325501.
[59] B Dorado, M Freyss, B Amadon, M Bertolus, G Jomard and P Garcia, Advances in first-principles modelling of point defects in UO_2: *f* electron correlations and the issue of local energy minima, J. Phys. Condens. Matter. 25 (2013) 333201.
[60] B. Dorado, B. Amadon, M. Freyss, M. Bertolus, DFT+U calculations of the ground state and metastable states of uranium dioxide, Phys. Rev. B Condens. Matter. 79 (2009) 235125.

Table 1. Fitted parameters for the Rose-Vinet equation of state. Data are presented at the reference temperature of 300K but can be used to estimate values at temperatures below the superionic transition.

	Rose-Vinet Parameters (values at T_R=300 K)			
Composition	Volume per formula unit / Å^3	Bulk Modulus / GPa	Derivative Bulk Modulus	Volume Expansivity / 10^{-5} K^{-1}
ThO_2	43.75	184.33	6.20	2.66
$U_{0.25}Th_{0.75}O_2$	42.99	188.91	6.69	2.77
$U_{0.50}Th_{0.50}O_2$	42.25	194.54	7.00	2.85
$U_{0.75}Th_{0.25}O_2$	41.56	198.85	7.17	2.90
UO_2	40.87	207.36	7.46	2.90
$Pu_{0.25}U_{0.75}O_2$	40.46	207.80	7.31	2.95
$Pu_{0.50}U_{0.50}O_2$	40.06	207.83	7.43	2.95
$Pu_{0.75}U_{0.25}O_2$	39.64	210.33	7.43	2.95
PuO_2	39.24	211.91	7.42	2.93

Table 2: Values of fitted parameters for the activation volume and thermal expansivity as a function of composition.

	$Th_{1-x}U_xO_2$		$U_{1-x}Pu_xO_2$	
	$\alpha(x,T_R)$	$c_{act}(x)$	$\alpha(x,T_R)$	$c_{act}(x)$
a_0	2.6583	0.304	2.90715	0.292
a_1	0.5676	–0.102	0.04159	–0.0612
a_2	–0.3188	–0.0206	-	0.0327
a_3	-	0.245	-	–0.0139
a_4	-	–0.133	-	-
D_0	-	0.45108	-	0.45108

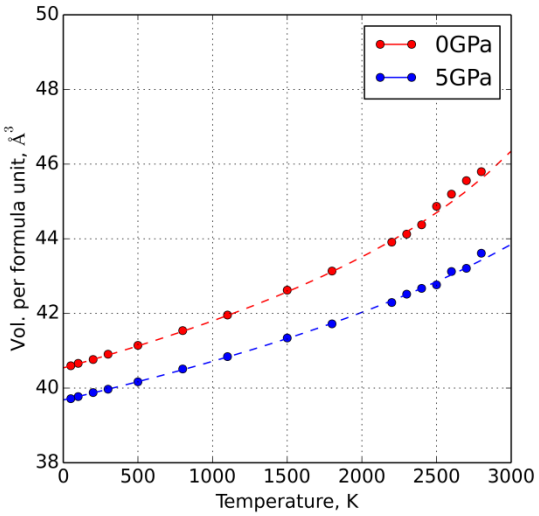

(a)i

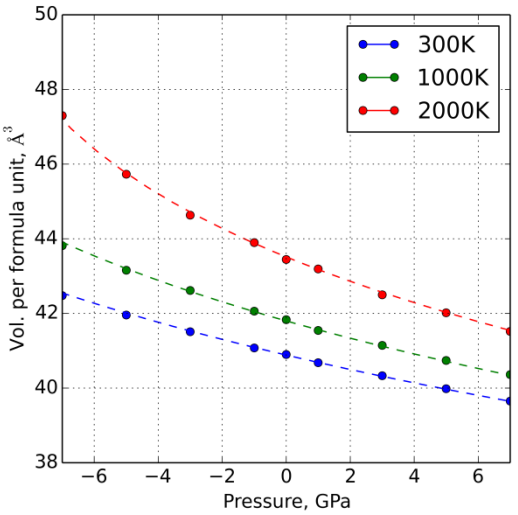

(a)ii

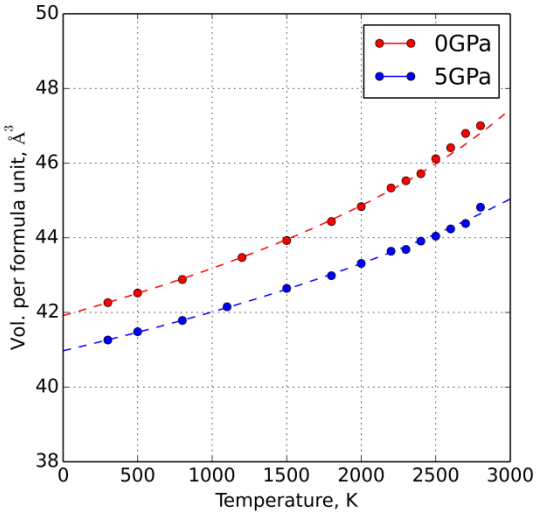

(b)i

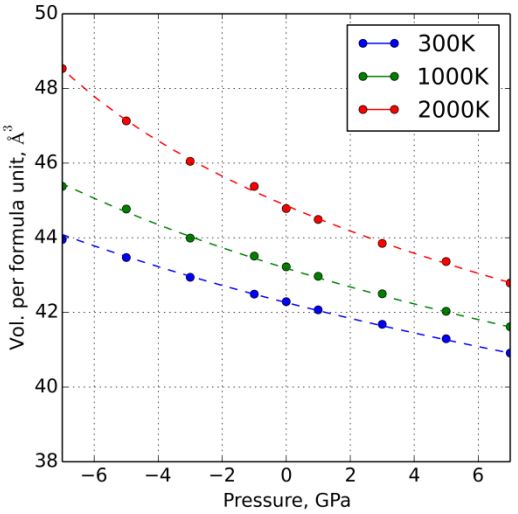

(b)ii

Figure 1: Plots of the predicted volume per formula unit against temperature (i) and pressure (ii) for (a) UO_2 and (b) $U_{0.5}Th_{0.5}O_2$. The dashed lines represent the Rose-Vinet fitted equation of state and the points are individual simulation results.

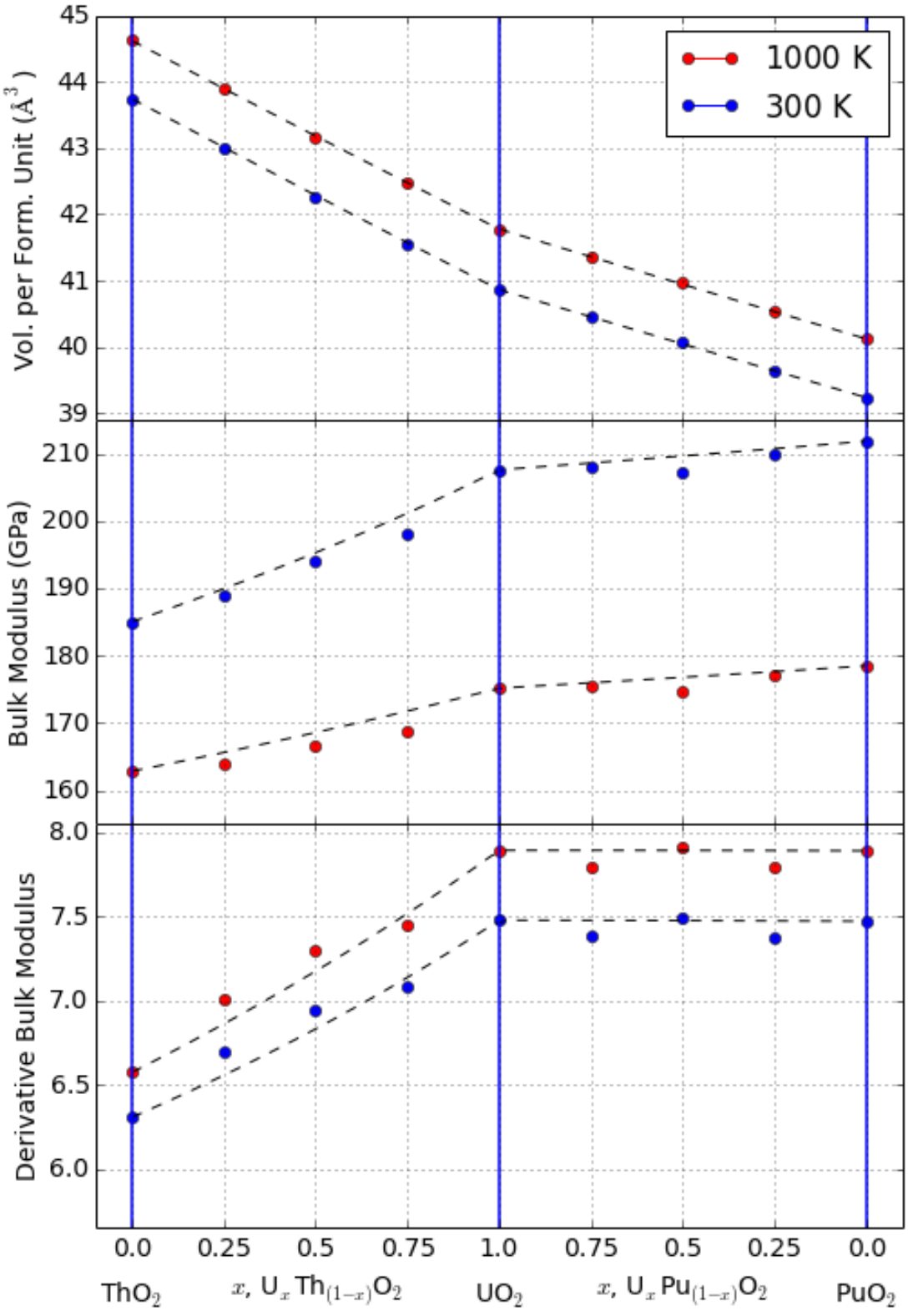

Figure 2: Plot of the value of bulk modulus calculated from the theoretical expression and fitting to the MD data.

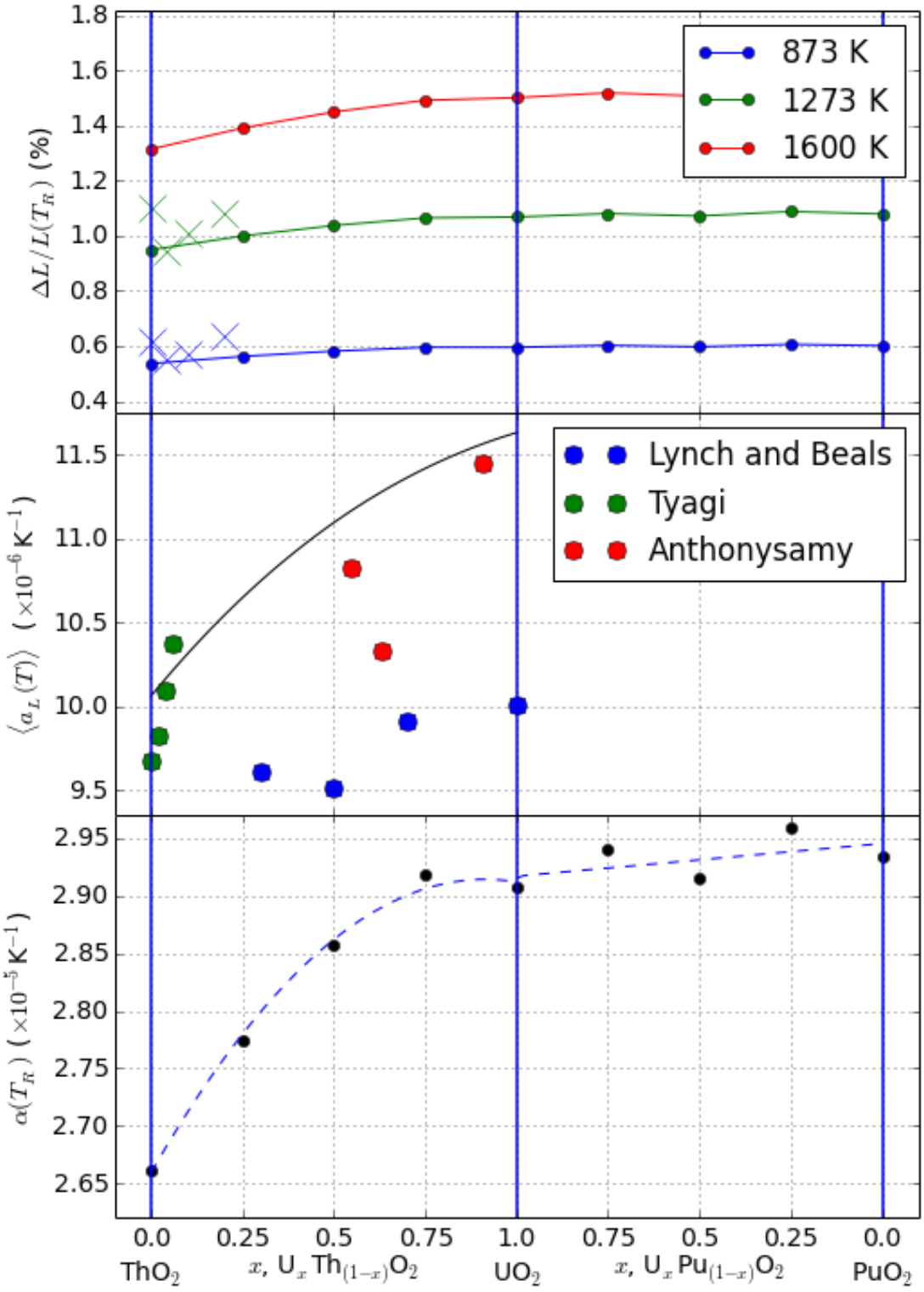

Figure 3: Plots showing the thermal expansion across a range of compositions. A common set of Rose-Vinet equations of state is used in all cases. The top plot shows the predictions at a range of temperatures and compared with experimental data [41] at 873K (blue crosses) and 1173K (green crosses); the middle plot shows the average thermal expansion between 293K and 1600K compared with data from References [46], [44,45] and [43]. The bottom plot shows the value of $\alpha(T_R)$ from Equation 4.

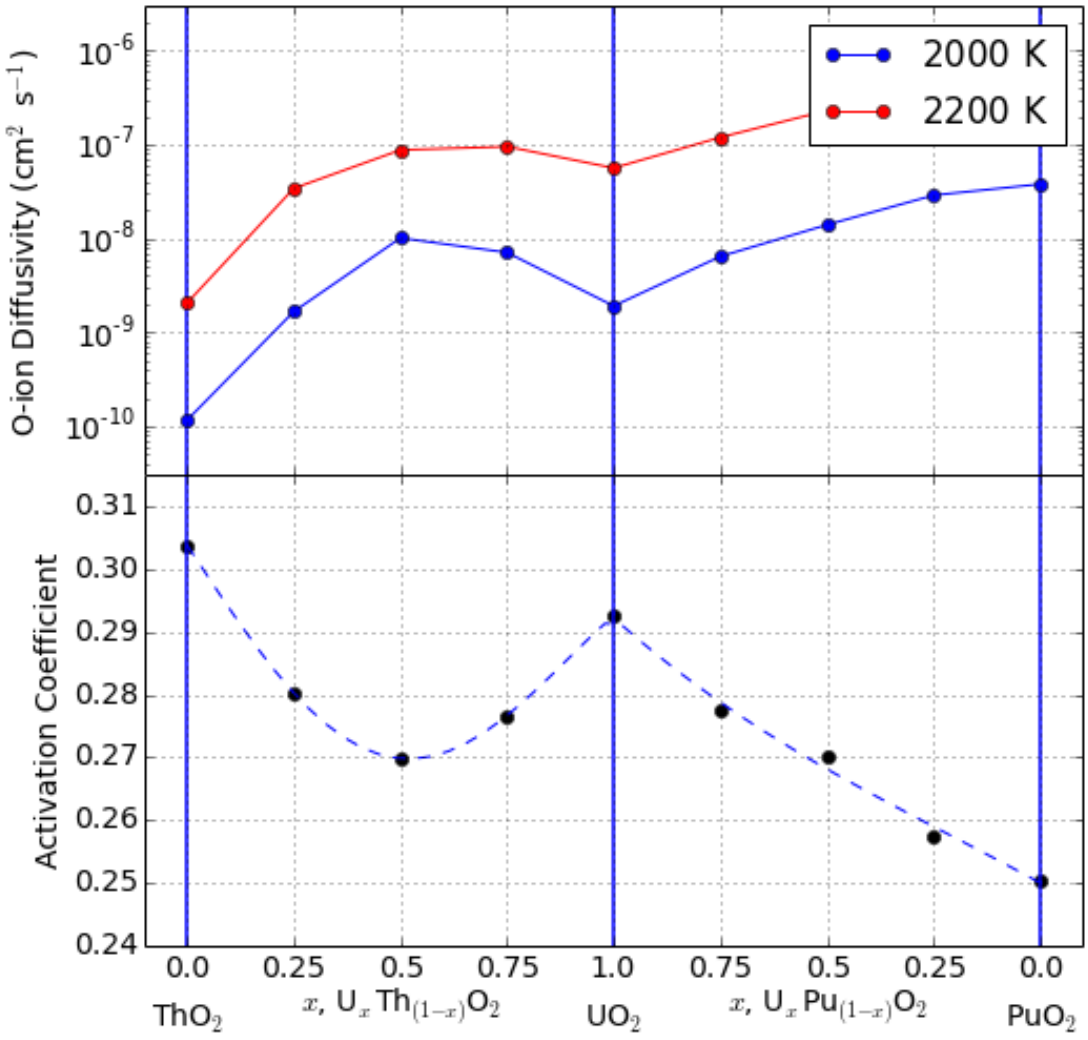

Figure 4: Plots showing the O-ion diffusivity and fitted values of the activation coefficient c_{act} as a function of oxide composition. The dashed lines show a polynomial fit to the data which is fourth-order for the $U_xTh_{1-x}O_2$ system and third-order for the $U_xPu_{1-x}O_2$ system.

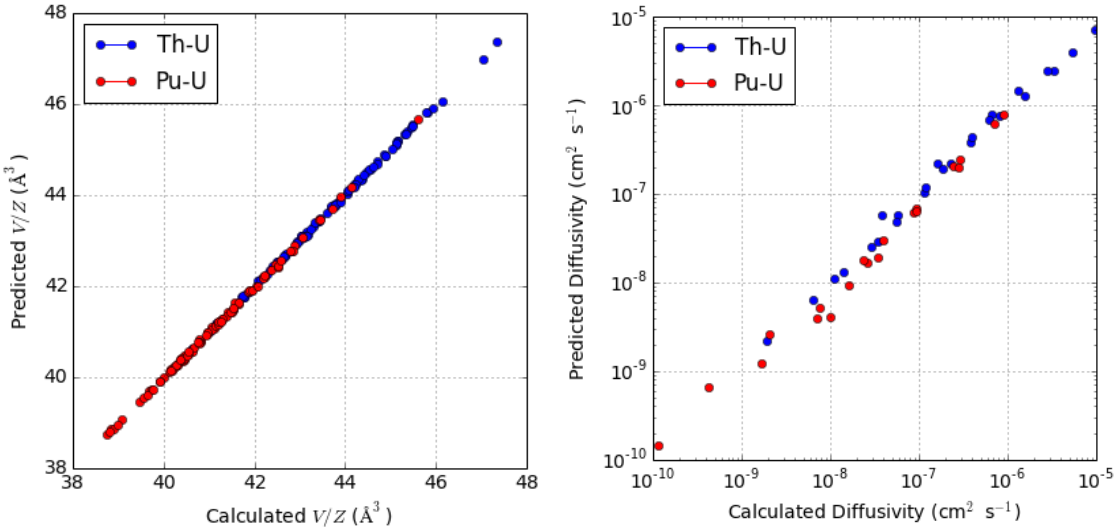

(a) (b)

Figure 5: Predicted and calculated values of the (a) volume per formula unit and (b) oxygen ion diffusivity for a range of different compositions.